

Intrinsic Images Decomposition Using a Local and Global Sparse Representation of Reflectance

Li Shen Chuohao Yeo
Institute for Infocomm Research

lshen@i2r.a-star.edu.sg

chyeo@i2r.a-star.edu.sg

Abstract

Intrinsic image decomposition is an important problem that targets the recovery of shading and reflectance components from a single image. While this is an ill-posed problem on its own, we propose a novel approach for intrinsic image decomposition using a reflectance sparsity prior that we have developed. Our method is based on a simple observation: neighboring pixels usually have the same reflectance if their chromaticities are the same or very similar. We formalize this sparsity constraint on local reflectance, and derive a sparse representation of reflectance components using data-driven edge-avoiding-wavelets. We show that the reflectance component of natural images is sparse in this representation. We also propose and formulate a novel global reflectance sparsity constraint. Using this sparsity prior and global constraints, we formulate a l_1 -regularized least squares minimization problem for intrinsic image decomposition that can be solved efficiently. Our algorithm can successfully extract intrinsic images from a single image, without using other reflection or color models or any user interaction. The results on challenging scenes demonstrate the power of the proposed technique.

1. Introduction

Intrinsic image decomposition addresses the problem of separating an image into its reflectance and shading components. This decomposition of intrinsic images is of importance in both computer graphics and computer vision applications. First, the intrinsic decomposition facilitates advanced image editing in graphics applications such as re-texturing, re-colorization and re-lighting. Second, the extracted intrinsic images benefit many computer vision algorithms. The shading images are preferred inputs to algorithms such as shape from shading. The reflectance images can be used for tasks such as segmentation and image white balance. Furthermore, most vision algorithms from low-level image analysis to high-level object recognition implica-

itly assume that its input image is a reflectance image.

However, recovering two intrinsic components from a single input image remains a challenging problem because of its severely ill-posed nature: given an input image that is the product of its reflectance and shading components, the number of unknowns is twice the number of equations.

1.1. Related Work

Intrinsic image decomposition was first introduced by Barrow and Tenenbaum [1]. The reflectance component describes the intrinsic albedo of a surface, which is illumination-invariant. The shading component corresponds to the amount of reflected light from the surface, which depends on surface geometry, reflection function and illumination condition.

Some previously proposed methods use additional information from multiple images to resolve the inherent ambiguities. For example, user registered images captured under different illumination conditions can be used [24, 16]. Such an approach can be extended to non-registered web image collections for applications such as colorizing grayscale images [15].

To overcome the severely ill-posed nature of the problem, previous methods for intrinsic image decomposition from a single image used a strong prior or assumption. Using the Retinex strategy [13, 11], Horn [9], and Funt and Drew [6] analyze local derivatives for distinguishing between image variations that are due to shading or reflectance. Their methods are based on the assumption that only large chromaticity changes are a result of reflectance changes, and that reflectance and shading changes do not coincide. Global optimization algorithms have also been proposed to obtain a global consistency of image structures [18, 20].

Training-based approaches have also been proposed to classify image derivatives into reflectance changes or shading changes [2, 22, 21]. With trained classifiers, Tappen et al. obtain good decomposition results by solving a global optimization problem with belief propagation [22]. However, the convergence of these systems are input dependent,

and there is little an end-user can do to control the final output.

More recently, a user-assisted method has been proposed by Bousseau et al. [3]. Focusing on diffuse objects, they use the assumption that local reflectance colors lie on a plane, and derive a closed-form least squares system which can be solved with additional user-supplied constraints. Their method obtains impressive results on the presented test images. However, their “color plane” assumption on local reflectance values is incompatible with many practical cases such as multicolor surfaces and the gray-scale input images.

1.2. Our Approach

In this paper, we propose a new prior on reflectance images for intrinsic image decomposition that is based on the following simple observation: if two neighboring pixels share similar chromaticity, it is very likely that they will have similar reflectance. Applying this insight on local reflectance, we derive a novel multi-scale sparsity prior on reflectance by applying a multi-resolution analysis using an data-driven edge-avoiding wavelet transform. We show that the reflectance component of natural images is *sparse* in such an appropriately chosen basis. By using a wavelet representation of reflectance, we formulate an ℓ_1 -regularized least-squares minimization problem for intrinsic image decomposition to solve for the reflectance component. The decomposition produced by our method is therefore the global optimum of a convex optimization problem.

We further make use of the assumption that natural images can be well-described by a small set of colors. We do this by formulating a global reflectance sparsity constraint that can be integrated into the earlier ℓ_1 -regularized least-squares minimization problem. We show that exploiting this assumption can lead to further improvements in our intrinsic image decomposition.

Our algorithm is independent of reflection/color models on local surfaces, and can obtain good separations on challenging reflection scenes.

2. A Sparse Representation for Reflectance

In this section, we show how to formulate and derive our sparse representation for the reflectance components of natural images using a simple local constraint on reflectance.

2.1. Reflectance Constraints

Our method is based on a simple observation: two neighboring pixels at locations i and j generally have the same reflectance if their chromaticities are very similar. As we will elaborate later, we can exploit this observation to build a local sparse representation of reflectance by minimizing

the following cost function:

$$J(R) = \sum_i \left\| R(i) - \sum_{j \in N_i} \widehat{w}_{ij} R(j) \right\|_1, \quad (1)$$

where $R(i)$ is the reflectance of pixel i , which is a RGB vector. N_i is the set of neighboring pixels of i and \widehat{w}_{ij} is a set of normalized non-negative weights which sum to one and is derived from w_{ij} (see (2) below). The weight should be large when the two chromaticities are similar, and small when they are different. The weighting function w_{ij} is based on the difference between the two chromaticities and the local chromaticity variance:

$$w_{ij} = \begin{cases} 0 & \text{if } \|C(i) - C(j)\| > t_c, \\ \exp\left(-\frac{\|C(i) - C(j)\|^2}{0.3\sigma_i^2}\right) & \text{otherwise.} \end{cases} \quad (2)$$

where $C(i) = R(i) / \|R(i)\|$ is the chromaticity of the reflectance at i and t_c is the threshold ($t_c = 0.02$ in our implementation). σ_i^2 is the chromaticity variance in a local window of 5×5 . Similar formulations to (2) have been used in image segmentation [19, 7] and colorization algorithms [14, 15]. However, in a twist from previous methods, while we use this formulation to enforce the local sparsity of reflectance, \widehat{w}_{ij} is computed using chromaticity.

2.2. Multi-resolution Analysis on Reflectance Distribution

Inspired by [4], we perform a multi-resolution analysis on reflectance images using the weighted red-black wavelets (RBW). RBW is a second generation wavelet first introduced by Uyttterhoeven et al. [23]. It is a two-step lifting construction for 2D signals that uses the quincunx lattices illustrated in Fig. 1. The pixels are first split into the red and black subsets (see Fig. 1a). Each black pixel is predicted using the four nearest red pixels, and the computed detail pixels, d^{k+1} , are stored at the black pixels. Then, the red pixels are updated using the computed detail coefficients stored at the black pixel locations. The red pixels are decomposed further into the blue and yellow subsets as shown in Fig. 1b. The yellow pixels are predicted using their four diagonally-located neighbors in the blue pixel locations, and the computed detail pixels, d^{k+1} , are stored at the yellow pixels. Finally, the blue pixels are updated using the computed detail coefficients stored at the yellow pixel locations, and the computed approximation coefficients, a^{k+1} , are stored at the blue pixels. Algorithm 1 presents the lifting scheme of the forward transform of the weighted RBW [4]. In this work, we perform $K = \lfloor \log_2(\min(x, y)) \rfloor$ levels of decomposition, where (x, y) is the image size. By inverting each of these lifting steps, the wavelet reconstruction can be obtained.

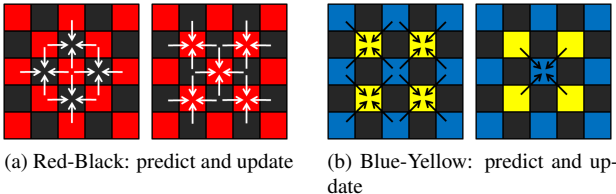


Figure 1: RBW construction. (a) illustrates the horizontal/vertical lifting in the Red-Black stage. (b) illustrates the diagonal lifting in the Blue-Yellow stage.

The predict and update steps of the Red-Black stage of the weighted RBW are defined by Equation (3) and Equation (4) respectively; the predict and update steps of the Blue-Yellow stage are similar and only differ in the neighborhood used. We can see that the predict operation is exactly the same as is used in the summation in Equation (1). By using as weights w_{ij} defined in Equation (2), weighted RBW transform provides us with a multi-resolution analysis tool on reflectance images. The update step of weighted RBW can be regarded as a chromaticity distribution preserving down-sampling. The coefficients \widehat{R} of reflectance component should be sparse since most of the detail coefficients, $\{d^k\}_{k=1}^K$, would be zero according to Equation (2).

Denote the weighted RBW forward transform operator by \mathcal{B}_w , and the backward transform operator by \mathcal{B}_w^{-1} . Then, the reflectance component of a natural image can be represented in the wavelet domain as:

$$\widehat{R} = \mathcal{B}_w R \quad (5)$$

where \widehat{R} are the wavelet coefficients of the reflectance.

In Fig. 2, we illustrate the coefficients obtained by our weighted RBW formulation, which is indeed very sparse. Our result is consistent with recent studies which show that the distribution of colors in natural scenes exhibits sparsity. Omer and Werman have shown that natural images can usually be described accurately using a small set of color lines in RGB space [17].

3. Recovering Intrinsic Images

Intrinsic image decomposition takes as input an image \mathcal{I} , which is modeled as a per-color-channel product of an reflectance component \mathcal{R} and an shading (illumination) component \mathcal{L} . We process these in the log domain. Denote by I , R and L the logarithms of \mathcal{I} , \mathcal{R} and \mathcal{L} , respectively. Thus, we are given:

$$I = R + L$$

and wish to recover R and L . Obviously, this is a severely under-constrained problem, since for each given pixel there are two unknowns. To solve this problem, further constraints are needed.

Input: Input image
Output: $a^K, \{d^k\}_{k=1}^K$

Initialize: Set the input image as a^0 ;

for $k \leftarrow 0$ to $K - 1$ **do**

Do Red-Black Stage **begin**

Split: Decompose a^k into the coarse data, $a_{C_{rb}}^k$, at locations C_{rb}^k (red) and fine data, $a_{F_{rb}}^k$, at locations F_{rb}^k (black)

Predict: Use $a_{C_{rb}}^k$ to predict $a_{F_{rb}}^k$

foreach $i \in F_{rb}^k$ **do**

$$d^{k+1}(i) = a_{F_{rb}}^k(i) - \sum_{j \in N_i} \widehat{w}_{ij} a_{C_{rb}}^k(j) \quad (3)$$

Update: Use d^{k+1} to update $a_{C_{rb}}^k$

foreach $i \in C_{rb}^k$ **do**

$$a_{C_{rb}}^k(i) = a_{C_{rb}}^k(i) + \frac{1}{2} \sum_{j \in N_i} \widehat{w}_{ij} d^{k+1}(j) \quad (4)$$

end

Do Blue-Yellow Stage **begin**

Split: Decompose $a_{C_{rb}}^k$ into coarse data, $a_{C_{by}}^k$, at locations C_{by}^k (blue), and fine data, $a_{F_{by}}^k$, at locations F_{by}^k (yellow)

Predict: Use $a_{C_{by}}^k$ to predict $a_{F_{by}}^k$

foreach $i \in F_{by}^k$ **do**

$$d^{k+1}(i) = a_{F_{by}}^k(i) - \sum_{j \in N_i} \widehat{w}_{ij} a_{C_{by}}^k(j)$$

Update: Use d^{k+1} to update $a_{C_{by}}^k$

foreach $i \in C_{by}^k$ **do**

$$a_{C_{by}}^k(i) = a_{C_{by}}^k(i) + \frac{1}{2} \sum_{j \in N_i} \widehat{w}_{ij} d^{k+1}(j)$$

end

Algorithm 1: Lifting scheme of weighted red-black wavelet

3.1. Basic Formulation

Assuming that the illumination component changes smoothly over the scene, we add a smoothness constraint on L . We would like to ensure that its Laplacian at all locations is small and formulate our smoothness cost on L as:

$$J_{\text{smooth}} = \sum_i \|\nabla^2 L(i)\|^2$$

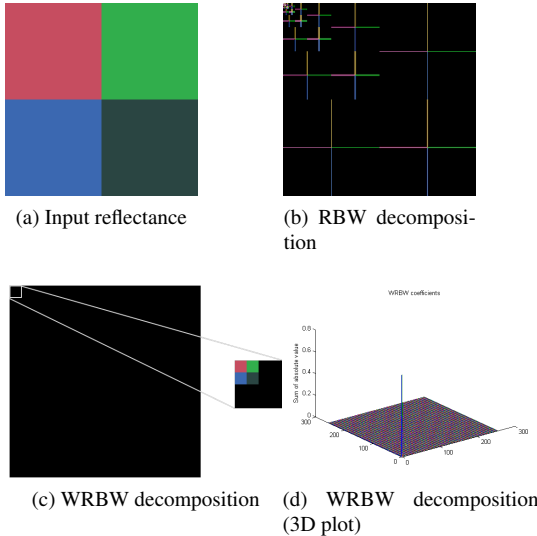


Figure 2: Illustration of sparse prior on reflectance. (a) Input reflectance. (b) Decomposition using the RBW constructed with equal weighting. (c) Decomposition using the WBRW constructed using chromaticity information from the input. Note the sparse nature of the coefficients, and the color-preserving down-sampling. (d) A 3D plot of the sum of absolute values of the WRBW coefficients (across RGB), further illustrating its sparse nature.

We add the smooth regularization of L to the system both to make sure that every pixels has an equation that constrains it, and to control the smoothness of the illumination component. The smoothness constraint also encourages the solution to interpolate over any gaps (e.g. the object boundaries) in the scene without introducing discontinuities.

Denote the Laplacian operator by Δ . We can express this smoothness constraint on the illumination with the following cost function:

$$\begin{aligned} J_{\text{smooth}} &= \|\Delta L\|^2 \\ &= \left\| \Delta I - \Delta \mathcal{B}_w^{-1} \hat{R} \right\|^2 \end{aligned}$$

To incorporate the requirement that \hat{R} is sparse and the smoothness constraint on illumination, we use a ℓ_1 -regularized least-squares [10] minimization framework. The smoothness constraint can be considered to be a set of measurements on the reflectance, i.e.,

$$(\Delta \mathcal{B}_w^{-1}) \hat{R} \approx \Delta I$$

Therefore, to recover a sparse \hat{R} , we would solve the following ℓ_1 minimization problem:

$$\min_{\hat{R}} \left\| \hat{R} \right\|_1 \text{ s.t. } A \hat{R} = y \quad (6)$$

where

$$A = \Delta \mathcal{B}_w^{-1} \text{ and } y = \Delta I \quad (7)$$

3.2. Reflectance weighting

We also want to weigh the reflectance coefficients, \hat{R} . According to Equation (3), when the surrounding chromaticities around a pixel are all very different, i.e., $w_{ij} = 0$ for all neighbors, \hat{R} stores the reflectance value of itself. The coarser the scale, the more frequently this will happen. Otherwise, the neighboring pixels have similar chromaticity, and \hat{R} stores the local reflectance differences. We wish to enforce the constraint that the reflectance difference of neighboring pixels with similar chromaticity is small. We do this by minimizing $\left\| \Lambda \hat{R} \right\|_1$, and applying a larger weighting at these locations, i.e.,

$$\Lambda_i = \begin{cases} \varepsilon & \text{if } w_{ij} = 0 \quad \forall j \in N_i, \\ 1 & \text{otherwise,} \end{cases}$$

recalling that N_i denotes the neighborhood set of location i . ε is a small value, which we set as 0.001 in our implementation.

Therefore, we obtain the following optimization from Equation (6).

$$\min_{\tilde{R}} \left\| \tilde{R} \right\|_1 \text{ s.t. } A \Lambda^{-1} \tilde{R} = y \quad (8)$$

where $\tilde{R} = \Lambda \hat{R}$.

3.3. Restricting the number of different reflectance values

Another constraint we would like to impose is that the total number of reflectance values (or colors) is small within the image. Omer and Werman [17] have shown that scenes are dominated by a small number of material colors. In other words, the set of reflectance spectra is sparse. We formulate this constraint by applying a total-variation cost on the set of reflectance values within the image. Recall from Equation (2) that when neighboring chromaticities are significantly different, the corresponding weights used in the weighted RBW are set to 0. This has the effect of retaining the actual reflectance value at that location and scale. When carrying out the initial wavelet decomposition, we keep track of this set of locations, Γ , where neighboring chromaticities are significantly different; we denote its cardinality by $M = |\Gamma|$. Let \mathcal{T} be the operator that computes all $\frac{M \times (M-1)}{2}$ differences between the reflectance values found in the locations stored in Γ . In other words, \mathcal{T} is a sparse matrix, except that for each possible combination of indices in Γ , one entry is created that corresponds to computing the difference between the reflectance values at the indices. For example, if the k th combination is between

index i and j , then $\mathcal{T}_{ki} = 1$ and $\mathcal{T}_{kj} = -1$. We would like $\mathcal{T}\hat{R}$ to be sparse. Therefore, we add an additional cost term to (8) to obtain:

$$\min_{\tilde{R}} \|\tilde{R}\|_1 + \|\mathcal{T}\Lambda^{-1}\tilde{R}\|_1 \text{ s.t. } A\Lambda^{-1}\tilde{R} = y \quad (9)$$

To solve (9), we introduce a slack variable, x , with the additional condition that $x = \mathcal{T}\Lambda^{-1}\tilde{R}$. Thus, the minimization now becomes:

$$\min_{\tilde{R},x} \|\tilde{R}\|_1 + \|x\|_1 \text{ s.t. } A\Lambda^{-1}\tilde{R} = y \text{ and } x = \mathcal{T}\Lambda^{-1}\tilde{R} \quad (10)$$

Re-writing this, we get:

$$\min_{\tilde{R},x} \left\| \begin{bmatrix} \tilde{R} \\ x \end{bmatrix} \right\|_1 \text{ s.t. } \begin{bmatrix} A\Lambda^{-1} & 0 \\ \mathcal{T}\Lambda^{-1} & -\mathcal{I} \end{bmatrix} \begin{bmatrix} \tilde{R} \\ x \end{bmatrix} = \begin{bmatrix} y \\ 0 \end{bmatrix} \quad (11)$$

Here, \mathcal{I} is the identity matrix.

3.4. Optimization

To perform the optimization, we use the following ℓ_1 -regularized least-squares problem formulation [10]:

$$\min_{\tilde{R},x} \left\| \begin{bmatrix} A\Lambda^{-1} & 0 \\ \mathcal{T}\Lambda^{-1} & -\mathcal{I} \end{bmatrix} \begin{bmatrix} \tilde{R} \\ x \end{bmatrix} - \begin{bmatrix} y \\ 0 \end{bmatrix} \right\|_2^2 + \lambda \left\| \begin{bmatrix} \tilde{R} \\ x \end{bmatrix} \right\|_1 \quad (12)$$

where the measurement matrix A and observation vector y are as in Equation (7), i.e., $A = \Delta\mathcal{B}_w^{-1}$ and $y = \Delta I$.

We use an interior-point method that solves the optimization problem given in (12) [10]. In particular, we take advantage of the fact that the A and A^T operators can be implemented efficiently without the need to perform full matrix multiplication. \mathcal{B}_w^{-1} can be computed using wavelet lifting, while \mathcal{B}_w^{-1T} can also be computed using wavelet lifting by choosing the right weights and switching the order of the predict and update steps. Λ is a diagonal matrix, Δ can be implemented with an image filter and \mathcal{T} is a sparse matrix with just 2 entries per row.

In our implementation, we use MATLAB code provided by Koh et al. [12] that performs the interior-point method using pre-conditioned conjugate gradients to solve for a good search direction during each update iteration. This approach has been shown to be more computationally efficient than competing methods, especially for large scale problems. The iterations are repeated until the target duality gap is reached. We use a relative tolerance of 0.01 on the duality gap, and set $\lambda = 0.001\lambda_{\max}$. λ_{\max} is the maximum value of λ for which the solution to optimization in Equation (12) does not converge to 0 (which is definitely sparse but otherwise not a meaningful solution) [10]. Typically, the smaller the value of λ , the sparser is the solution vector.

4. Experimental Results

We first test our algorithm using the MIT dataset [8] which offers a ground-truth dataset of intrinsic images decompositions of 16 real objects. In the experiments, we test two algorithm. First, we only use the sparsity constraint on the WRBW representation of reflectance (SR) in the algorithm which solves (6). Then, we use both the global constraint on reflectance color, and the sparse representation constraint of reflectance (SRC), and solve (11). We quantitatively verify the correctness and performance of our algorithm by computing the Local Mean Squared Errors (LMSE) [8] of our separation results. As indicated in [8], with single image, color Retinex (CR) [5] has the best performance among the intrinsic image algorithms which uses local constraints. We compare our methods, SR and SRC, with CR. The LMSE values of the whole dataset used for comparisons are computed using the Color Retinex algorithm made available by the MIT Intrinsic Images [8].¹

Table 1 shows the decomposition results of the compared methods for an instance of each category in the MIT dataset. CR correctly identifies most of the markings as reflectance changes for the case of raccoon and cup1. However, it still leaves some “ghost” markings in the shading and some residue of the cast shadows in the reflectance images. SR eliminates many of these residue. The turtle is a difficult example in the dataset, because shading and reflectance changes are inter-mixed. It is hard to estimate the decomposition using local information. Our reflectance representation is driven from the Retinex local constraint. However, the global sparsity constraint on the representation broadens the influence of local cues to help resolve the ambiguous local inferences. SR successfully separates the reflectance and shading on the shell. By employing the global constraint of reflectance color, SRC better preserves the global shading reflectance structures of the turtle. Another example is shown in Figure 3. SRC effectively eliminates cast shadows found inside the box from the reflectance.

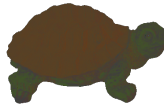
Table 2 shows the LMSEs of our methods compared with CR for all 16 objects. SR outperforms CR for most of the objects, and SRC generally has the best performance. Since LMSE estimates local error up to a scale, it fails to capture the global structure of reflectance and shading. Some intrinsic decomposition results of SRC exhibit better global consistency even though the LMSE scores are similar.

4.1. Comparison with user-assisted approaches

Our proposed global sparsity constraint on reflectance colors preserves global consistency of the reflectance and shading structures in a scene. In this section, we compare our method with that of Bousseau et al. [3] Bousseau et al.

¹Some of the computed values could be a little different from that presented in [8] because of the convergence algorithm.

Table 1: Decomposition results by color Retinex and our approach on three images from the MIT intrinsic dataset

	Raccoon	Cup1	Turtle
Image			
GT	 	 	 
CR	  $LMSE = 0.015$	  $LMSE = 0.007$	  $LMSE = 0.069$
SR	  $LMSE = 0.0052$	  $LMSE = 0.0043$	  $LMSE = 0.035$
SRC	  $LMSE = 0.0048$	  $LMSE = 0.0042$	  $LMSE = 0.0174$

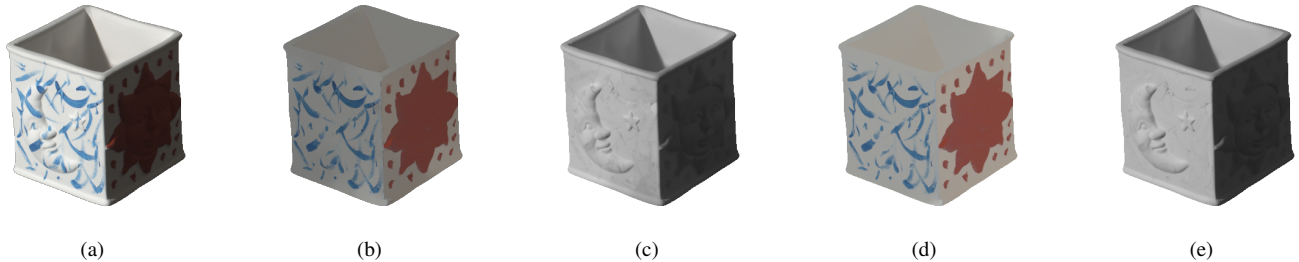


Figure 3: Intrinsic image decomposition result. (a) Input image. (b-c) Separated reflectance and shading images using the sparsity constraint on the WRB wavelets components of reflectance ($LMSE = 0.003606$). (d-e) Results after adding the global sparsity constraint on reflectance color ($LMSE$ is 0.001835)

Table 2: Statistics of LMSEs of our methods and color Retinex for all the images

	box	cup1	cup2	frog1	frog2	panther	paper1	paper2	raccoon	sun	teabag1	teabag2	turtle	Ave.
CR	0.013	0.007	0.011	0.066	0.071	0.011	0.004	0.004	0.015	0.003	0.032	0.023	0.069	0.025
SR	0.0036	0.0043	0.0052	0.0558	0.0587	0.0075	0.0019	0.0027	0.0052	0.0024	0.0280	0.0151	0.0349	0.017
SRC	0.0018	0.0042	0.0050	0.0526	0.0435	0.0078	0.0014	0.0027	0.0048	0.0023	0.0268	0.0151	0.0174	0.015

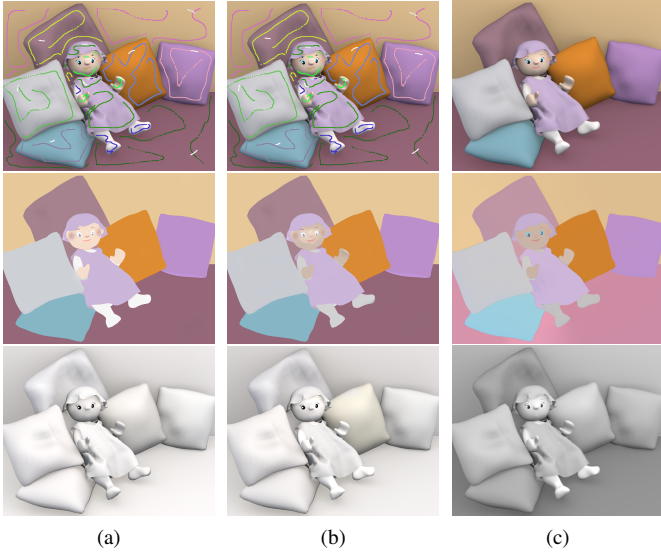


Figure 4: Comparison with Bousseau’s approach. (a) Bousseau’s results when user strokes are set to ground truth values ($\text{LMSE} = 0.00055$). (b) Bousseau’s results when the positions of user strokes are randomly perturbed by up to 15 pixels ($\text{LMSE} = 0.0011$). (c) Our results without user interaction ($\text{LMSE} = 0.0015$).

use the following global constraints provided by a user: sets of pixels with similar reflectance, sets of pixels with similar illumination, and locations and shading values of pixels with known illumination. Accurate decomposition results can be achieved by using the global constraints of shading and reflectance provided in the form of user scribbles. However, users may not always provide useful scribbles. Figure 4 shows the decomposition results with ground truth scribbles (Figure 4a), with perturbed user scribbles (Figure 4b), and our proposed method without any user interaction (Figure 4c). The fixed illumination values of the scribbles in Figure 4b are set to ground truth values, but with a position randomly perturbed by up to 15 pixels. The LMSE of our method is 0.0015, while the LMSE of Bousseau et al.’s method is 0.0011 using the scribbles with the small variation in positions. Our method generate visually comparable results without additional information. Figure 5 shows more comparisons with the method proposed by Bousseau et al.

5. Conclusions

In this paper, we have described a novel approach for intrinsic image decomposition based on a data-driven sparse representation of reflectance that we have developed. A sparse representation is made possible by using edge-avoiding weighted red-black wavelets constructed with chromaticity information from the input image. At the same time, the constructed weighted red-black wavelet also preserves chromaticity distribution even at coarse scales. We formulate the decomposition as a ℓ_1 -regularized least-squares minimization problem, and seek to recover the sparse reflectance signal given smoothness constraints on the illumination component. Further improvements are demonstrated by using a global assumption that the number of different colors is small through the use of a total-variation like approach.

Our results show that such an approach can decompose complex natural images. The results of our decomposition can then be used as inputs for down-stream applications such as re-texturing and segmentation.

References

- [1] H. Barrow and J. Tenenbaum. Recovering intrinsic scene characteristics from images. *Computer Vision Systems*, pages 3–26, 1978. [697](#)
- [2] M. Bell and W. T. Freeman. Learning local evidence for shading and reflectance. In *IEEE Int’l Conf. on Computer Vision (ICCV)*, volume 1, pages 670–677, 2001. [697](#)
- [3] A. Bousseau, S. Paris, and F. Durand. User-assisted intrinsic images. In *SIGGRAPH Asia ’09: ACM SIGGRAPH Asia 2009 papers*, pages 1–10. ACM, 2009. [698](#), [701](#)
- [4] R. Fattal. Edge-avoiding wavelets and their applications. *ACM Trans. Graph.*, 28(3):1–10, 2009. [698](#)
- [5] G. D. Finlayson, S. D. Hordley, and M. Drew. Removing shadows from images using retinex, 2002. [701](#)
- [6] B. V. Funt, M. S. Drew, and M. Brockington. Recovering shading from color images. In *European Conf. on Computer Vision (ECCV)*, pages 124–132, 1992. [697](#)
- [7] L. Grady. Random walks for image segmentation. *IEEE Trans. on Pattern Analysis and Machine Intelligence*, 28(11):1768–1783, 2006. [698](#)
- [8] R. Grosse, M. K. Johnson, E. H. Adelson, and W. T. Freeman. Ground-truth dataset and baseline evaluations for intrinsic image algorithms. In *International Conference on Computer Vision*, pages 2335–2342, 2009. [701](#)
- [9] B. K. P. Horn. *Robot Vision*. MIT Press, 1986. [697](#)

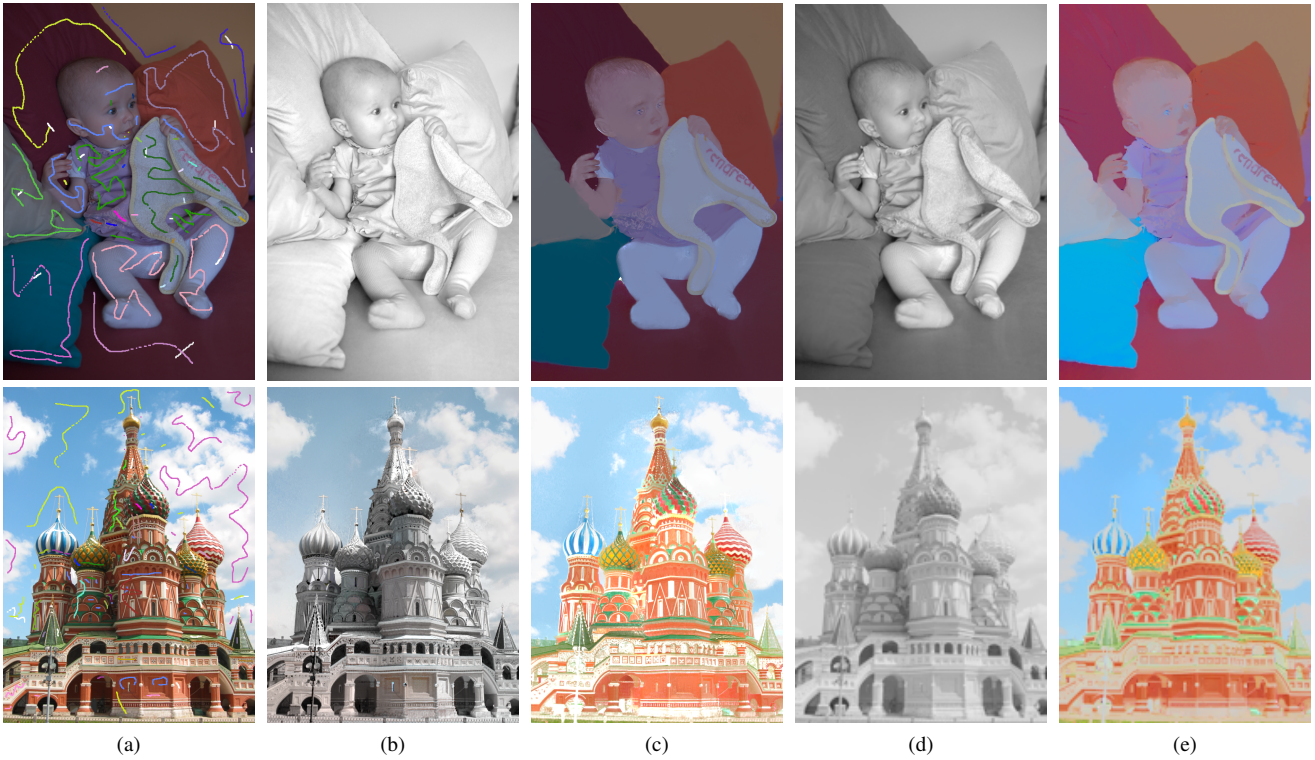


Figure 5: Comparison with Bousseau’s approach. (a) User scribbles used by Bousseau’s method (b-c) Bousseau’s results. (d-e) Our results without any user interaction

- [10] S.-J. Kim, K. Koh, M. Lustig, S. Boyd, and D. Gorinevsky. An interior-point method for large-scale l_1 -regularized least squares. *IEEE Journal on Selected Topics in Signal Processing*, 1(4):606–617, 2007. [700](#), [701](#)
- [11] R. Kimmel, M. Elad, D. Shaked, R. Keshet, and I. Sobel. A variational framework for retinex. *International Journal of Computer Vision*, 52:7–23, 2003. [697](#)
- [12] K. Koh, S.-J. Kim, and S. Boyd. l_1 l_s : Simple matlab solver for l_1 -regularized least squares problems. http://stanford.edu/~boyd/l1_ls.html, 2008. [701](#)
- [13] E. Land and J. McCann. Lightness and retinex theory. *Journal of the Optical Society of America A*, 3:1684 – 1692, 1971. [697](#)
- [14] A. Levin, D. Lischinski, and Y. Weiss. Colorization using optimization. 23(3):689–694, 2004. [698](#)
- [15] X. Liu, L. Wan, Y. Qu, T.-T. Wong, S. Lin, C.-S. Leung, and P.-A. Heng. Intrinsic colorization. *ACM Transactions on Graphics (SIGGRAPH Asia 2008 issue)*, 27(5):152:1–152:9, December 2008. [697](#), [698](#)
- [16] Y. Matsushita, S. Lin, S. B. Kang, and H.-Y. Shum. Estimating intrinsic images from image sequences with biased illumination. In *European Conf. on Computer Vision (ECCV)*, volume 2, pages 274–286, 2004. [697](#)
- [17] I. Omer and M. Werman. Color lines: Image specific color representation. *Computer Vision and Pattern Recognition*, *IEEE Computer Society Conference on*, 2:946–953, 2004. [699](#), [700](#)
- [18] L. Shen, P. Tan, and S. Lin. Intrinsic image decomposition with non-local texture cues. In *CVPR*, pages 1–7, 2008. [697](#)
- [19] J. Shi and J. Malik. Normalized cuts and image segmentation. *IEEE Trans. on Pattern Analysis and Machine Intelligence*, 2000. [698](#)
- [20] P. Sinha and E. Adelson. Recovering reflectance and illumination in a world of painted polyhedra. In *IEEE Int’l Conf. on Computer Vision (ICCV)*, pages 156–163, 1993. [697](#)
- [21] M. Tappen, E. Adelson, and W. Freeman. Estimating intrinsic component images using non-linear regression. In *IEEE Conf. on Computer Vision and Pattern Recognition (CVPR)*, pages II: 1992–1999, 2006. [697](#)
- [22] M. F. Tappen, W. T. Freeman, and E. H. Adelson. Recovering intrinsic images from a single image. *IEEE Trans. on Pattern Analysis and Machine Intelligence*, 27:1459–1472, 2005. [697](#)
- [23] G. Uytterhoeven and A. Bultheel. The Red-Black wavelet transform. In M. Moonen, editor, *Signal Processing Symposium (IEEE Benelux)*, pages 191–194. IEEE Benelux Signal Processing Chapter, 1998. [698](#)
- [24] Y. Weiss. Deriving intrinsic images from image sequences. In *IEEE Int’l Conf. on Computer Vision (ICCV)*, volume 2, pages 68–75, 2001. [697](#)